QWIPs at IRnova, a status update

Henk Martijn, Anders Gamfeldt, Carl Asplund, Sergiy Smuk, Himanshu Kataria, Eric Costard
IRnova AB Electrum 236, SE-164 40 Kista, Sweden

ABSTRACT

IRnova has a long history of producing QWIPs for the LWIR band. In this paper we give an overview of the current products (FPAs with 640x480 and 384x288 pixels respectively, and 25 µm pitch) and their performance. Their superior stability and uniformity inherent to detectors based on III/V material system will be demonstrated. Furthermore, an IDCA specifically designed for hand-held systems used for the detection of SF_6 gas using a 0.5 W cooler will be presented. The detector format is 320x256 pixels with 30 µm pitch using the ISC9705 read out circuit. The peak wavelength is at 10.55 µm and the NETD is 22 mK.

Keywords: QWIP, LWIR, gas, SF_6

1. INTRODUCTION

IRnova has a long track record in the development and production of Quantum Well Photo Detectors (QWIPs). IRnova's production has its basis in early QWIP research[1,2,3]. Since the start of production in the year 2000 more than 3000 high quality detectors have been shipped and production volumes are increasing (Figure 1a). QWIPs, based on the mature III/V material system AlGaAs/GaAs, have shown very good uniformity, operability and stability. This is particularly a strong advantage in the LWIR band, where the competing technology MCT (Mercury Cadmium Telluride) is struggling with these specific issues and where the lower quantum efficiency of QWIPs doesn't pose a problem due to the abundance of photons available. The high quality of the final product is in large part due to control over the whole manufacturing chain: from the in-house growth of the detector material to the semiconductor process and the final measurements, which makes rapid feedback on quality possible.

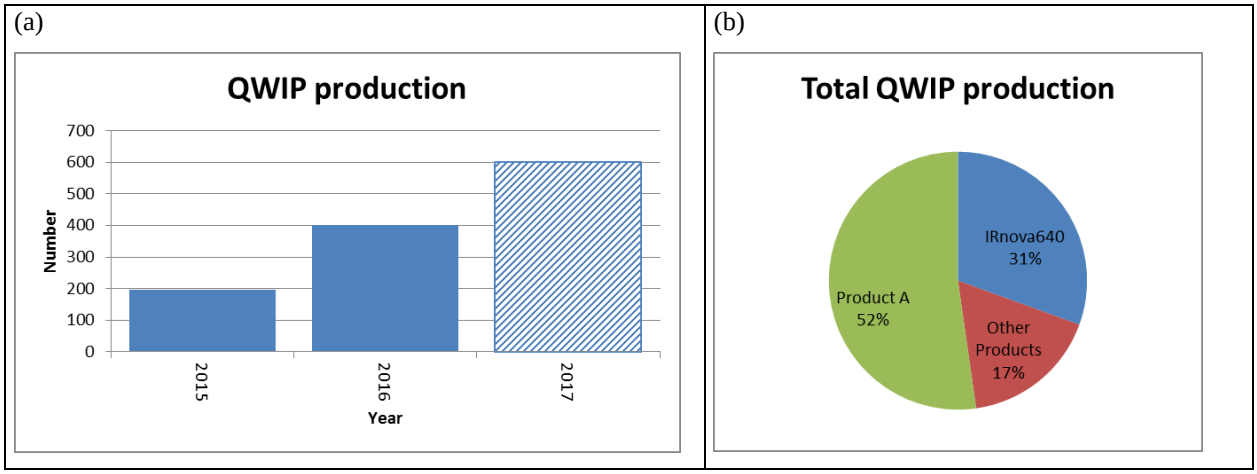

Figure 1. (a) QWIP production volumes from 2015 and onwards and (b) Distribution of the historical QWIP production over several products

In this paper, results from the epitaxial growth of MQW (Multi Quantum Well) structures will be shown with focus on uniformity and reproducibility. The high quality of the MQW wafer is a prerequisite for the efficient and stable production of the QWIP FPAs. The superior stability and uniformity will be shown of FPAs with different formats and peak wavelength. One of these detectors is IRnova640, a detector in VGA format. The production volume of this detector is almost 1/3rd of the total historic production volume of QWIPs at IRnova (Figure 1b). Finally we will report on the excellent results of the modification of a standard LWIR QWIP to a detector with a peak wavelength at 10.55 µm; specifically targeting the gas detection market.

2. EPITAXIAL GROWTH OF MQW

High quality detector material is mandatory for the efficient production of QWIP focal plane arrays. Metal-Organic Vapor Phase Epitaxy (MOVPE) is presently a well-established technology for GaAs based optoelectronic device production. The industrial process of today, with high demands on reproducibility in combination with increasing production volumes, requires high uniformity. MOVPE can fulfil these requirements far more competitively in terms of cost, than Molecular Beam Epitaxy.

In this paper we will demonstrate the level of performance that can be reached for some key material parameters like doping and thickness variations, both over a wafer ("spatial uniformity"), as well as over time (between wafers in a growth campaign and between campaigns).

2.1 Method

The MOVPE growth is performed on semi-insulating 4" GaAs substrates in a vertical EMCORE D-180 rotating disc reactor. Trimethylgallium, trimethylaluminium and arsine are employed as precursors in hydrogen carrier gas at a total pressure of 100 mbar and growth temperature of 700°C. Disilane is used as n-type doping source. Layer thicknesses and therefore growth rates are determined by X-ray diffraction (XRD) measurements. Net carrier concentrations are estimated by Hall measurements. As a measure of the electro-optical performance of the material so-called edge polished devices are fabricated and both dark current and responsivity vs temperature are measured.

The growth of production quality QWIP wafers is organized in growth campaigns. These campaigns start off by the calibration of the machine: growth rates and doping levels and their uniformity over the substrate are established. In the next step a full structure (trial wafer) is grown. This wafer is processed into single-pixel edge polished devices and electro-optical characterization is performed. If this evaluation gives results according to specification the real production campaign starts. Each individually produced wafer is subjected to quality control (morphology and XRD). The last wafer of the production campaign is again verified for its electro-optical performance.

2.2 Results and discussion

During the calibration phase of the machine the different doping levels (n-type doping in the contacts and quantum wells) are calibrated. Figure 2 shows the net carrier concentration per QW period for a typical wafer. The net carrier concentration is determined by the balance of intentionally added Si (n-type) and residual C (p-type) from incomplete decomposition of the metalorganic Al precursor molecules. The decomposition of the Si precursor molecule Si_2H_6 is complete at the growth temperature, whereas the incorporation of residual C (of the order of 10^{-5} per Al atom) is strongly reduced with increasing growth temperature. The measured net carrier concentration uniformity over the wafer is used to adjust the growth temperature between different radial zones of the wafer. The net doping uniformity over a wafer reached is better than ± 5 %.

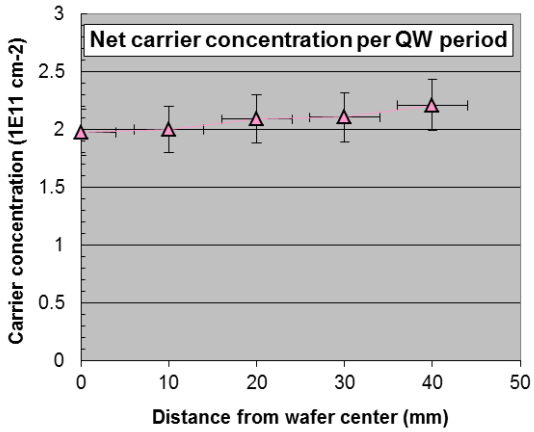

Figure 2. Net carrier concentration over the radius of a 4" wafer at 5 different positions

The growth temperature is high enough that the Ga and Al precursors which reach the wafer surface are 100 % decomposed – the growth rate is mass transport limited. This means that the growth rate is governed by the concentration of source material, while at the same time being insensitive to local temperature variations. The reactor used has several different inlets for the precursors into the chamber and by changing the flow distribution between these the uniformity of the growth rate can be controlled. A radial thickness uniformity measurement of a MQW structure is shown in Figure 3. The maximum deviation is less than 0.9 % over the wafer and is a proof of the suitability of MOVPE as technology of choice for the growth of MQWs.

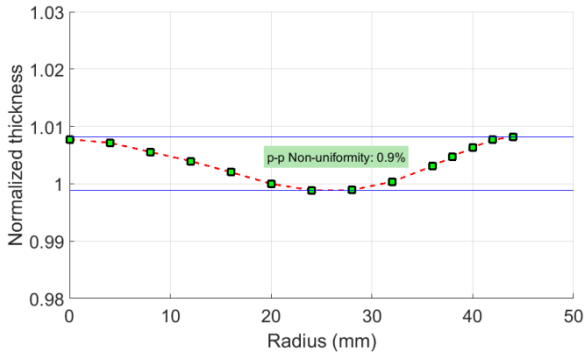

Figure 3. Normalized thickness uniformity of a MQW-structure measured radially with XRD

In Figure 4 the thickness variation of one period of an MQW-structure from run to run in a campaign and between campaigns is demonstrated. Only production runs of the same structure-design are included in this graph. The expected thickness is 435 Å. The actual thicknesses were deduced by means of XRD. We see a thickness variation in the range of ±3 Å per period between runs; this corresponds to a variation of just a bit more than one monolayer (ML).

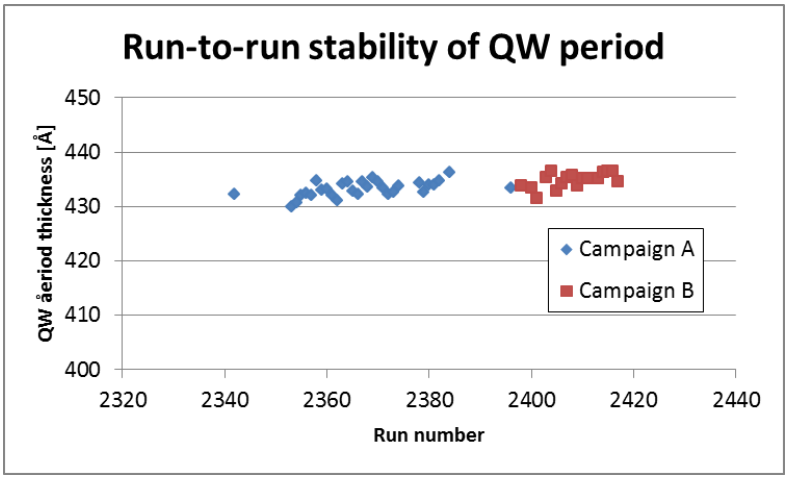

Figure 4. Thickness deviation of one period of an MQW-structure from run to run

In Figure 5, the responsivity and dark current density is shown of three fully processed wafers coming from the same EPI campaign. There are only very minor differences from wafer to wafer in responsivity (both peak wavelength and absolute value) and dark current.

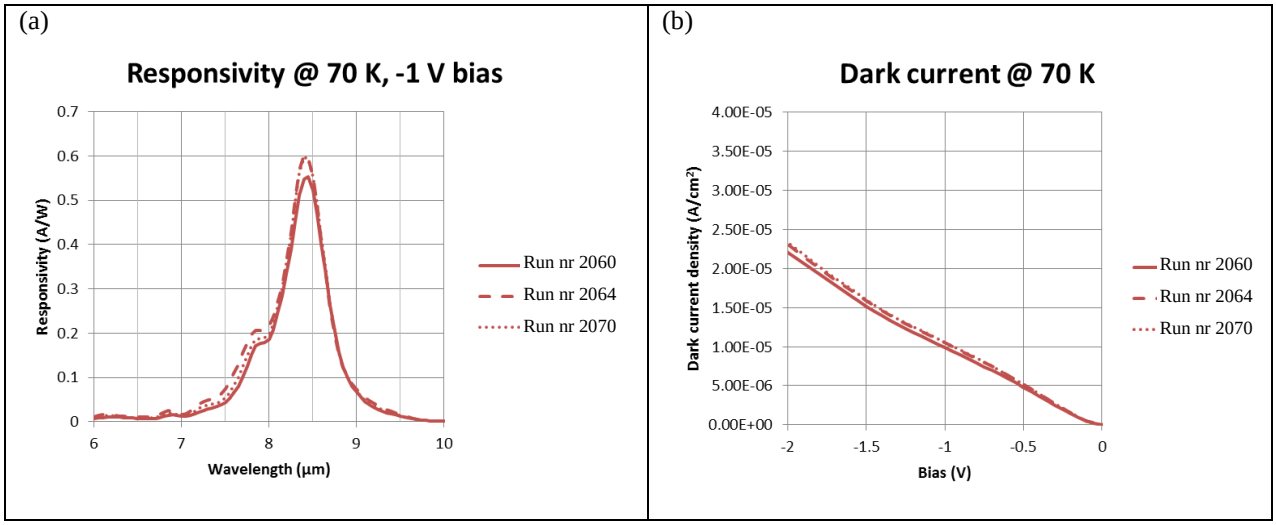

Figure 5. (a) Responsivity and (b) Dark current density for three different wafers of the same EPI campaign, measured at 70 K. Run numbers 2060, 2064 and 2070 are respectively from the beginning, middle and end of the EPI campaign.

2.3 Conclusions

The growth of industrial quality MQW structures with MOVPE is well established. The absolute net doping concentration deviation can be kept within ± 5 % over a whole wafer. Spatial uniformity of the thickness is reached with a variation of less than 0.9 %. The reproducibility of the same parameter is ± 3 Å from run to run. This high uniformity of basic parameters over the wafer is the key for producing FPAs that exhibit high image quality and show low variations in response and dark current from unit to unit. This will be shown in Figure 7.

3. DETECTOR PERFORMANCE

3.1 Test Method

Radiometric performance testing is carried out on each produced detector to examine its compliance with the specification.

The FPA, fitted on a ceramic carrier, is mounted on a cold finger in a test Dewar: an openable vessel suitable for active vacuum pumping equipped with a high performance Stirling cooler. The Dewar is fitted with a window that is transparent to infrared light (normally, germanium). The aperture is defined by a cold shield adjusted for the particular type of product to be characterized.

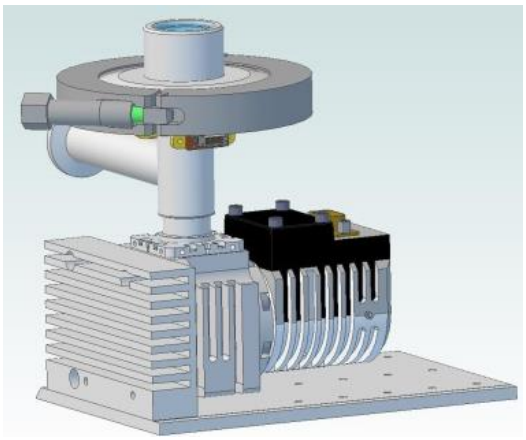

Figure 6. Test Dewar used for the radiometric testing of FPAs

The Dewar with the detector is mounted into a measurement station equipped with a number of targets. At IRnova there are 4 blackbodies with regulated, stabilized temperature, a special blackbody with stabilized temperature below room temperature and a mirror.

3.2 IRnova 384-ER FPA

IRnova384-ER is a quarter VGA FPA based on ISC0208 ROIC. The main characteristics and typical performance are shown in Table 1.

Table 1. Characteristics and typical performance of IRnova384-ER FPA

Parameter	**Value**	**Comment**
Array format	384 x 288	
Pixel pitch	25 µm	
ROIC	ISC0208	
Temporal NETD mean	28 mK	F/2.7 cold shield, 70 K operating temperature 100 % well fill corresponds to: 70 °C
Spatial NETD mean	11 mK	
Responsivity	19 mV/K	
Integration Time	4.5 ms	
Operability	99.97 %	A pixel is considered non-operating if: • Responsivity ± 30 % of the global mean Responsivity • NETD > 110 mK

As a method to evaluate the quality of a wafer, but also as a tool to find and identify potential production problems, the responsivity over a whole wafer is reconstructed. To this end, a field-of-view corrected responsivity map of each detector is placed in its right location on the wafer. The results of such a reconstruction can be seen in Figure 7a. The intrinsic detector efficiency is a measure of the sensitivity of the detector and is directly proportional to the quantum efficiency of the FPA. It is calculated by dividing the median of all pixel responsivity in mV/K by the integration time. In Figure 7b the intrinsic detector efficiencies of detectors from the same wafer are shown. The variation is ±13 % and is a proof that the EPI growth and the III/V process are very uniform. From both figures one can really appreciate the benefits of a mature III/V process: it leads to stable production and high production yields.

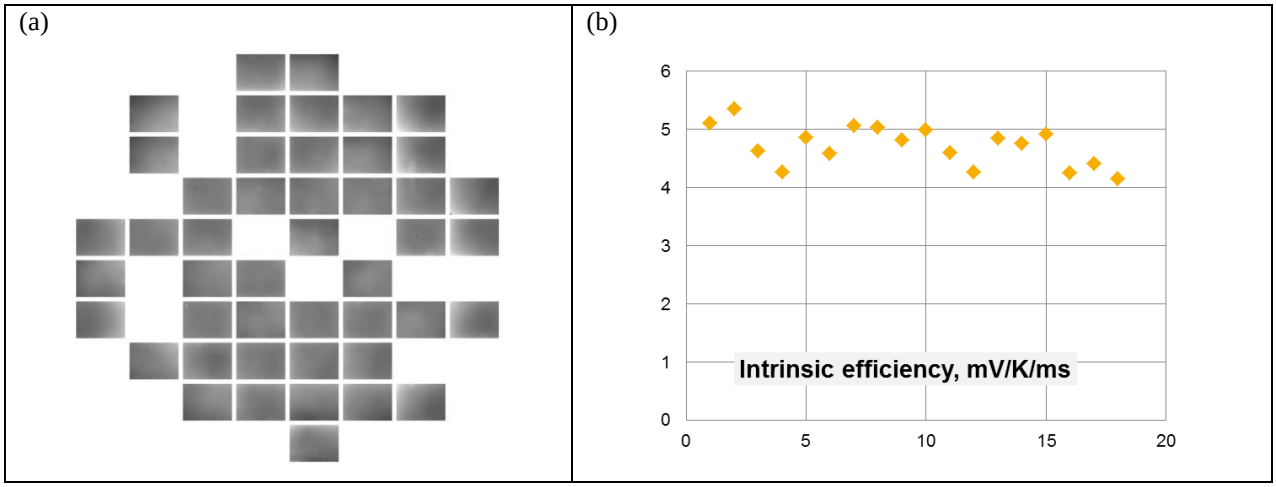

Figure 7. (a) reconstructed wafer map, each sub image represents the field of view corrected responsivity, the grey scale corresponds to ± 10% of the mean image value (b) variation of the intrinsic detector efficiency of detectors from the same wafer

The correctability and image stability of the IRnova384-ER has been studied. A prerequisite of a stable detector is that the distribution of the temporal noise of all pixels does not show a large tail. An example of a histogram of the noise in all pixels can be seen in Figure 8. The spatial noise has been studied to assess the image stability of the QWIP detector. Spatial noise is a statistical measure of how much pixels deviate from their neighbours. To calculate the spatial NETD a series of non-uniformity corrected (NUC) images are taken of a black body with a temperature half way between the two black body temperatures used for the NUC (30 °C and 50 °C in this case). The median value in time of each pixel is then

calculated to generate a single image (minimizing the effect of temporal noise). This image is then divided into blocks of 5×5 pixels, and the standard deviation of all pixel values in each block is calculated. The spatial NETD is the median of all these standard deviation values, divided by the response per Kelvin. Here, the spatial NETD is presented as ratio of the temporal NETD. In Figure 9a, the spatial NETD versus black body temperature is shown after an initial measurement and repeated after a temperature cycle of the FPA. Between the two correction points the spatial noise is less than 40 % of the temporal noise. Even outside the correction points the spatial noise does not exceed the temporal noise. Even over time the image stability is excellent, as can be concluded from Figure 9b: the spatial NETD is constant during the one hour long measurement.

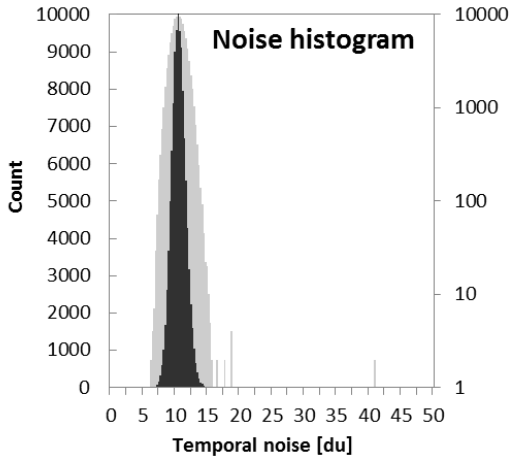

Figure 8. Distribution of the temporal noise of all pixels of an array when looking at a blackbody of 30 °C. black: linear scale, grey: log scale

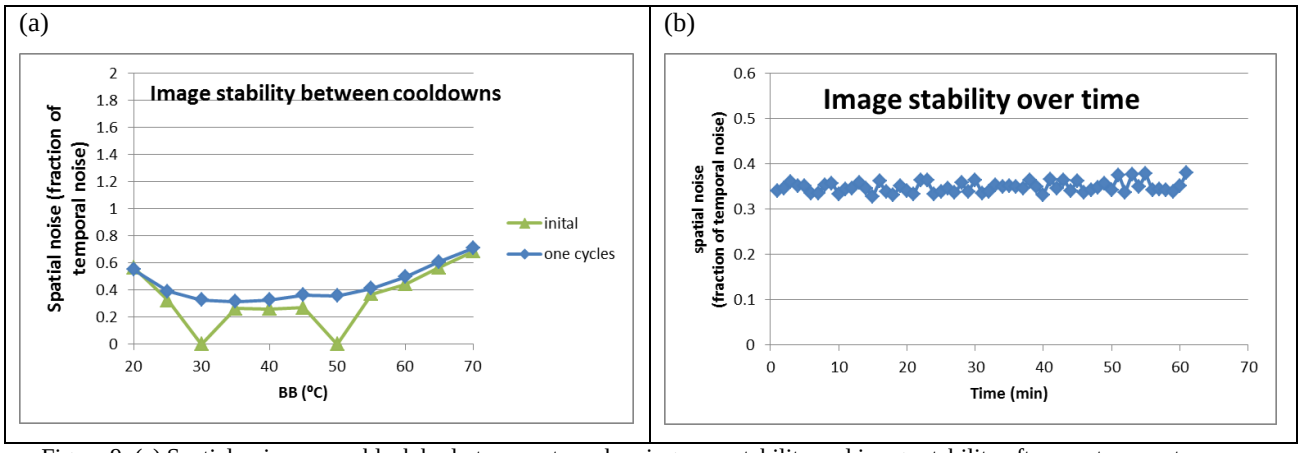

Figure 9. (a) Spatial noise versus black body temperature showing correctability and image stability after one temperature cycle (2-point corrections were performed at 30 °C and 50 °C). (b) Spatial noise versus time. 2-point correction performed with the same gain and offset map derived from measurements at t = 0

3.3 IRnova640 FPA

The IRnova640 FPA is a detector in production since the year 2001. It is a VGA format detector particularly suited for surveillance and security applications due to the crisp and stable imagery it provides. The main features of this product are summarized in Table 2.

Table 2. Characteristics and typical performance of IRnova640 FPA (measured over a large production interval)

Parameter	**Value**	**Comment**
Array format	640 x 480	
Pixel pitch	25 µm	
ROIC	Argus640	Proprietary ROIC
Temporal NETD mean	35 mK	F/2.7 cold shield, 100 % well fill corresponds to: 80°C
Spatial NETD mean	13 mK	
Integration Time	6.6 ms	
Operability	99.87 %	A pixel is considered non-operating if: • Responsivity deviates > ± 5 % of its neighbours • Temporal NETD > 120 mK • Spatial NETD: deviate more than 150 mK from its neighbours after non uniformity correction

When we look at a production run of one variant of this product (with a specific MQW design) we can plot both the temporal NETD and operability. The size of the population in question is 512 units. As can be seen in Figure 10b, the NETD is stable around 35 mK, with a variation of only ±5 mK. The operability statistics shown in Figure 10c are calculated with the non-operating pixel criteria defined in Table 2. The mean operability in this population is 99.87 %. These are of course excellent results, especially when keeping in mind that this is a relative large VGA sized detector and is a further proof of the excellent production properties of III/V material. No other IR detector technology can come near this type of performance in the LWIR region.

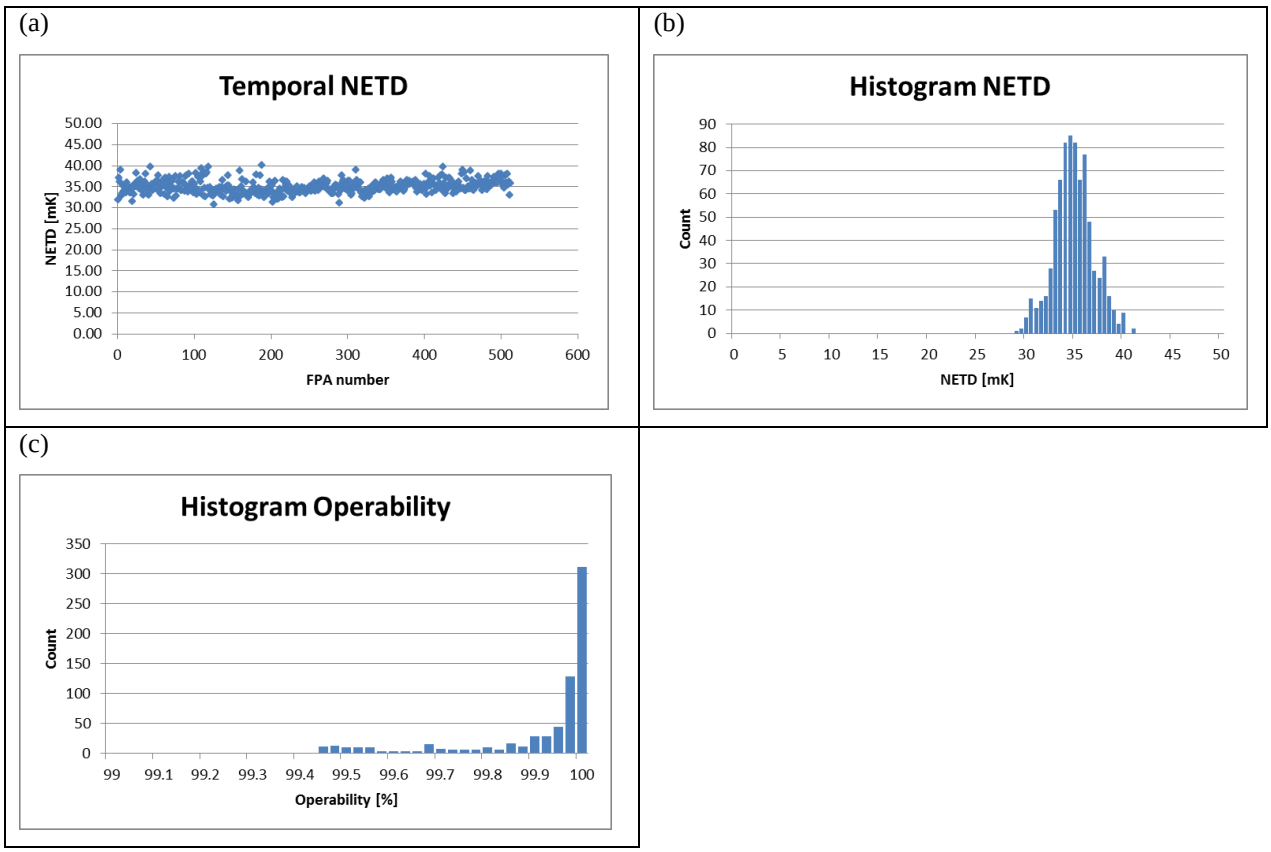

Figure 10. (a) Temporal NETD for more than 500 production quality FPAs (b) Distribution of the NETD from the same population (c) Distribution of the operability; were a pixel is declared as non-operating pixel according to definition in Table 2

3.4 Gas leak detection

All gas leak detection is based on the absorption of specific wavelengths in various gases making them visible to customized IR detectors. This enables imaging of gas leaks at safe distances and quick surveying of large areas.

To maximize the sensitivity of a detector for a specific gas, the spectral band of detection needs to be matched to the absorption band of the gas of interest. This minimizes the amount of out-of-band signal that gives no information on the amount of gas in sight, thus maximizing the relevant signal-to-noise ratio. For a QWIP this band matching is straight forward as a QWIP has inherently a narrow spectral response.

Several gases have absorption peaks very near to each other, which enables the use of a single detector system for detection of a large set of different gases. Some wavelength regions of interest are depicted in Figure 11.

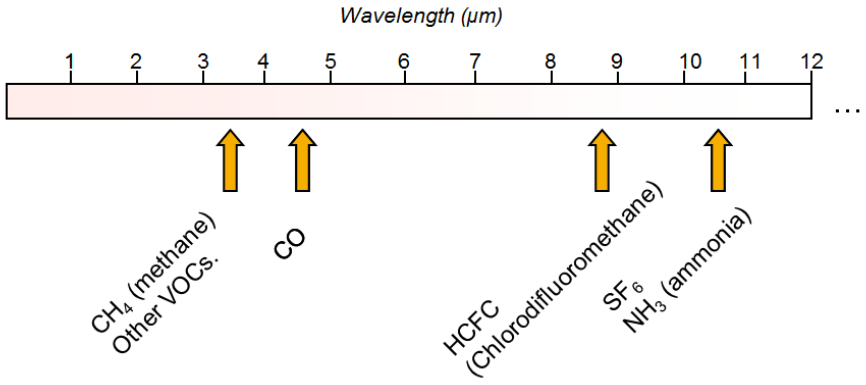

Figure 11. Absorption peaks of some different gases

In the mid wave infrared range there is a large group of volatile organic compounds (VOC), for example methane, butane and propane with peaks around 3.3 µm that can be detected. For these gases a T2SL detector can be used, as reported in ref [5]. In the long-wave infrared range sulphur hexafluoride (SF_6) and ammonia (NH_3) can be detected with a peak at 10.55 µm[6]. In this paper, we will show the performance of a QWIP specifically designed for this wavelength and statistics of the latest production runs.

To modify a standard LWIR QWIP design with peak wavelength at 8.5 µm to a peak wavelength of 10.55 µm is straight forward and requires only an adjustment of the MQW structure and a tuning of the grating period to optimize the light coupling to the required wavelength. No changes in the production processes are needed, demonstrating the robustness of an III/V detector and the ease of tailoring the wavelength of a QWIP.

3.5 IRnova320-ER 10.55, FPA

The FPA used for gas detection has a format of 320×256 pixels and uses the ISC9705 ROIC. More details are shown in Table 3.

Table 3. Characteristics and typical performance of IRnova320-1055 FPA

Parameter	Value	Comment
Array format	320 x 256	
Pixel pitch	30 µm	
ROIC	ISC9705	
Peak wavelength	10.55 µm	
Temporal NETD mean	24 mK	F/2.0 cold shield, 56 K operating temperature 100 % well fill corresponds to: 50 °C Measured with narrow cold filter around 10.55 µm
IntegrationTime	9.4 ms	
Operability	99.88 %	A pixel is considered non-operating if: • Responsivity deviates > ± 7.5 % of its neighbours • Temporal NETD > 120 mK • Spatial NETD: deviate more than 80 mK from its neighbours after non uniformity correction

The spatial and temporal noise of a detector fabricated with this MQW design is shown as function of detector temperature in Figure 12. Below 56 K the performance does not change significantly. This allows the use of a 500 mW cryocooler, hence making the IDCA compatible with a hand held camera.

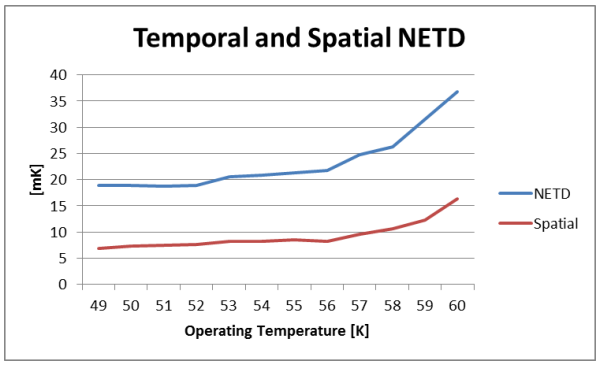

Figure 12. Temperature dependence of the temporal and spatial NETD from 49 to 60 K

Statistics from a run of 140 fabricated FPAs (Figure 13 a & b) show a stable and reproducible temporal NETD distribution around 24 mK.

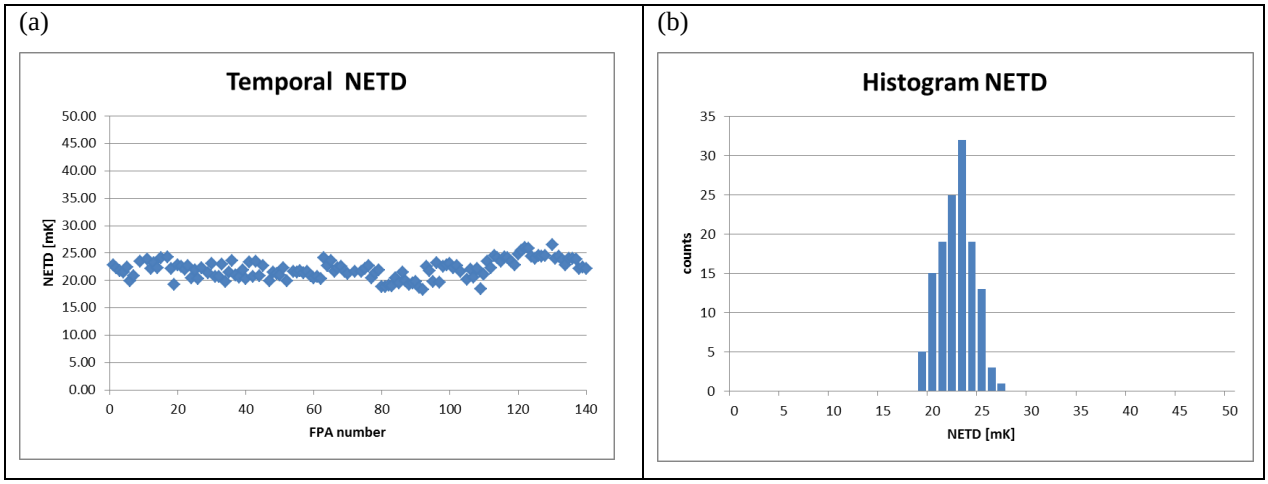

Figure 13. (a) Temporal NETD for 140 production quality FPAs and (b) Distribution of the NETD from the same population

The tested FPAs (Figure 14a) are integrated in an IDCA as shown in Figure 14b. An example of a complete hand held camera build based on an IRnova detector is shown in Figure 14c. In the image below (Figure 14 (d), taken at a detector operating temperature of 56 K), we see clearly the SF_6 gas leaking out of a tube. The gas has a lower temperature than its background and due to the absorption band around 10.55 µm we can observe the presence of the gas. Smart temporal algorithms can be applied to enhance the visibility of the gas in the image.

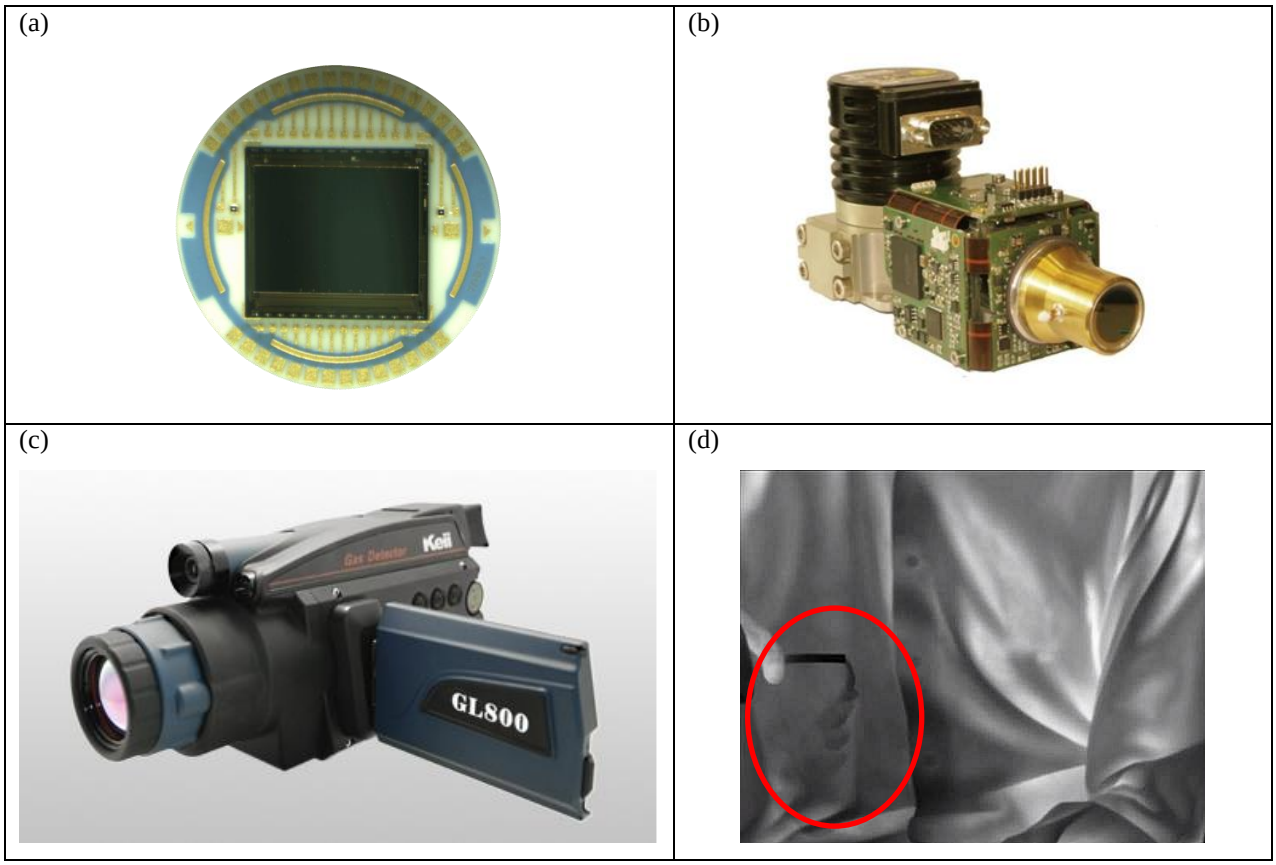

Figure 14. (a) Photo of a IRnova 10.55 FPA on ceramic carrier (b) Photo of IRnova 10.55 DDCA (c) Keii Camera with an IRnova 10.55 DDCA inside, Courtesy of Keii) (d) Image with an IRnova-ER10.55 FPA at 56 K with escaping Sulphur Hexafluoride in the circle

4. SUMMARY

As we have shown, QWIPs are a very good choice for high performance LWIR imaging. The starting point of an efficient production is good detector material. MOVPE can deliver detector wafers with the needed uniformity and run-to-run stability of key parameters. The superior uniformity and stability of QWIPs have been demonstrated based on production statistics of several products. The spatial noise remains low after a temperature cycle of the detector and no negative effects on the image quality could be observed. A production run of more than 500 detectors in the VGA format show a mean operability of 99.87 % and a low spread of the NETD. Adjusting the wavelength of a standard LWIR QWIP to fit the requirement of a gas sensing application has been shown to be straight forward and require only a design change of the MQW and grating. No changes in the production process are needed.

5. ACKNOWLEDGEMENTS

The authors would like to thank all the personnel of IRnova for their efforts in performing this work.

REFERENCES

[1] Andersson, J. Y. and Lundqvist, L., "Near-unity quantum efficiency of AlGaAs/GaAs quantum well infrared detectors using a waveguide with a doubly periodic grating coupler," Appl. Phys. Lett. 59, 857-859 (1991).

[2] Andersson, J. Y. and Lundqvist, L., "Grating coupled quantum well infrared detectors: Theory and performance," J. Appl. Phys. 71, 3600-3610 (1992)

[3] Lundqvist, L., Andersson, J. Y., Paska, Z. F., Borglind, J., and Haga, D., "Efficiency of grating coupled AlGaAs/GaAs quantum well infrared detectors, " Appl. Phys. Lett. 63, 3361-3363 (1993).

[4] Martijn, H. H., Smuk, S., Asplund, C., Malm, H., Gromov, A., Alverbro, J., Bleichner, H., ”Recent advances of QWIP development in Sweden,” Proc. SPIE 6542, 65420V-1-10 (2007).

[5] Malm, H., Gamfeldt, A., Marcks von Würtemberg, R., Lantz, D., Asplund, C. and Martijn, H., “High Image Quality Type-II Superlattice Detector for 3.3 µm Detection of Volatile Organic Compounds,” Infrared Physics & Technology, Volume 70, 34-39 (2015)

[6] http://www.ir-nova.se/applications/gas-detectionindustrial/